INTERNATIONAL ATOMIC ENERGY AGENCY
UNITED NATIONS EDUCATIONAL, SCIENTIFIC AND CULTURAL ORGANIZATION

INTERNATIONAL CENTRE FOR THEORETICAL PHYSICS
34100 TRIESTE (ITALY) - P.O.B. 586 - MIRAMARE - STRADA COSTIERA 11 - TELEPHONES: 224281/2/3/4/5/6
CABLE: CENTRATOM - TELEX 460392-I

SMR/113 - 17

AUTUMN COLLEGE

ON

THE TROPOSPHERE, STRATOSPHERE AND MESOSPHERE

10 September - 19 October 1984

MICROWAVE DUCT PROPAGATION OVER THE SEA

S. ROTHERAM

Marconi Research Centre
West Hanningfield Road
Great Baddow
Chelmsford, Essex
U.K.

MICROWAVE DUCT PROPAGATION OVER THE SEA

S. Rotheram

Marconi Research Centre, U.K.

INTRODUCTION

Radio waves propagating close to the earths surface are strongly affected by atmospheric conditions giving rise to evaporation, advection and subsidence ducts. Models are given for evaporation and advection ducts but subsidence ducts are only described qualitatively. Field strength calculations involve geometrical optics, waveguide mode and parabolic equation methods. Finite difference mode methods are being developed for elevated ducts and parabolic equation methods for horizontally varying media. Waveguide mode calculations in the evaporation duct over a rough sea are presented and are in qualitative agreement with data.

EVAPORATION DUCTS

These are shallow overwater surface ducts of order 5-15 m thick. At the sea surface the air is saturated but not usually at higher levels. This gives an approximately logarithmic decrease of water vapour pressure with height and is the primary cause of the evaporation duct. Close to the sea surface the modified and potential refractive indices m and n_p are related by

$$m = n_p + \frac{z}{Ka} \tag{1}$$

where z is height, a is the earth's radius and K = 1.205 at the sea surface. Over small height intervals

$$n_p - n_{po} = c(e_p - e_{po}) + f(\theta - \theta_o) \tag{2}$$

$$c = \frac{.373}{T^2}\ ,\ f = -7.76 \times 10^{-5}\frac{P}{T^2} - .746\frac{e}{T^3} \tag{3}$$

where e_p is the potential vapour pressure, θ is the potential temperature, T is temperature, e is vapour pressure, P is pressure, and n_{po}, e_{po} and θ_o are the surface values. The theory of the constant flux surface layer is given by the Monin-Obukhov similarity theory (1). If s is θ, e_p or horizontal wind speed u, then

$$s - s_o = \frac{s_*}{\varkappa\alpha_s}\int_o^z \frac{dz\varphi_s(z/L)}{z + z_s} = \frac{s_*}{\varkappa\alpha_s}\left[\ell n\left(\frac{z+z_s}{z_s}\right) + \psi_s(z/L)\right] \tag{4}$$

$$s_*u_* = -\langle s'w'\rangle\ ,\ \frac{1}{L} = \frac{\varkappa g}{T}\frac{(\theta_* + .38Te_*/P)}{u_*^2} \tag{5}$$

in which L is the Monin-Obukhov stability length, s_o is the surface value of s, s_* is a scale for s, s' and w' are the fluctuations in s and w, and w is the vertical wind speed.

If c and f are treated as constants, eqns.(2) and (4) show that s can stand for n_p with $n_* = ce_* + f\theta_*$. From measurements made by Businger et al (2)

$$\varkappa = .35,\ \alpha_u = 1,\ \alpha_\theta = \alpha_e = \alpha_n = 1.35 \tag{6}$$

$$\varphi_u(x<0) = (1-15x)^{-\frac{1}{4}}\ ,\ \varphi_u(x>0) = 1 + 4.7x \tag{7}$$

$$\varphi_\theta(x<0) = (1-9x)^{-\frac{1}{2}}\ ,\ \varphi_\theta(x>0) = 1 + 6.5x \tag{8}$$

$$\varphi_\theta(x) = \varphi_e(x) = \varphi_n(x) \tag{9}$$

The ψ_s forms are found from eqn. (4). The z_s are related to neutral drag coefficients by $C_s^{\frac{1}{2}} = \varkappa\alpha_s/\ell n(z/z_s)$. For z = 10 m, Kondo (3) gives $C_\theta = C_e = C_n = 1.3 \times 10^{-3}$ whilst $C_u \times 10^3$ is .96, 1.2, 1.4 and 1.8 when u = 2.2, 5, 8 and 25 m/s. Combining eqns. (1),(2) and (4) gives for the m-profile

$$m - m_o = \frac{1}{Ka}\left[z - \frac{d}{\varphi_n(d/L)}\int_o^z \frac{dz\varphi_n(z/L)}{z + z_n}\right] \tag{10}$$

$$d = -\frac{n_*}{\varkappa\alpha_n}\,Ka\varphi_n(d/L) \tag{11}$$

where d is the duct thickness. The m-profile depends upon the two parameters d and L. Figure 1 shows it as a single family of curves with $10^6(m-m_d)/d$ plotted against z/d for various values of d/L, where $m_d = m(d)$. One can determine d and L from simple measurements of u, θ and e_p at height z and surface temperature θ_o, with e_{po} the saturation vapour pressure at θ_o and $u_o = 0$. With $\zeta = z/L$, L is found from

$$\zeta_o = \frac{\varkappa gz}{T}\frac{C_\theta^{\frac{1}{2}}}{C_u}\left[\theta - \theta_o + .38T(e_p - e_{po})/P\right] \tag{12}$$

$$\zeta = \zeta_o\frac{[1 + \psi_u(\zeta)/\ell n(z/z_u)]^2}{[1 + \psi_\theta(\zeta)/\ell n(z/z_\theta)]} \tag{13}$$

ζ_o is found from the measurements and ζ, and hence L, is then found by inverting eqn.(13) either graphically or by a simple algorithm. The scales s_*, including n_*, are found from eqn. (4) using the measured $s - s_o$ and calculated L. The duct thickness d is then found by inverting eqn. (11). This method is sensitive to experimental errors. Wet and dry bulb, or equivalent, measurements must be made to .1°C and this is difficult in a marine environment. Similarity theory breaks down in strongly stable conditions and this increases sensitivity to errors. The theory is useless for d/L>.07. Information exists on evaporation duct statistics. Figure 2 shows mean values in metres for European waters. Monthly means of d(m) are strongly correlated with θ_o(°C) with $d \sim 1 + .4\,\theta_o$.

ADVECTION DUCTS

The passage of warm well mixed air from land over a cooler sea leads to a modified layer near the surface within which humidity decreases while temperature increases with height forming an advection duct. In a model given by Mulhearn (4), θ, e_p, n_p and u assume constant values θ_1, e_{p1}, n_{p1} and u_1 in the well mixed air mass over the land, and θ_o, e_{po} n_{po} and 0 at the sea surface. Over the sea a modified layer of height z_m grows with wind fetch x with the empirical form

$$\frac{z_m}{L_m} = .014\left(\frac{x}{L_m}\right)^{.55} \tag{14}$$

$$\frac{1}{L_m} = \frac{g}{u_1^2}\left[\frac{\theta_1 - \theta_o}{\theta_1} + \frac{.38(e_{p1} - e_{po})}{P}\right] \tag{15}$$

where L_m is a bulk stability parameter. Within the modified layer θ, e_p and n_p vary like $z^{\frac{1}{4}}$ so the m-profile and duct thickness d are

$$m - m_o = \frac{z}{Ka} + (n_{p1} - n_{po})\left[H(z-z_m) + H(z_m - z)\left(\frac{z}{z_m}\right)^{\frac{1}{4}}\right] \tag{16}$$

$$d = z_m \min\left[1, \left\{(n_{po} - n_{p1})\frac{Ka}{4z_m}\right\}^{\frac{4}{3}}\right] \tag{17}$$

where H(.) is the unit step function. Figure 3(a) shows experimental M-profiles given by Unwin (5) whilst figure 3(b) shows $M - M_o = 10^6(m - m_o)$ from eqn. (16) with $10^6(n_{po} - n_{p1}) = 30$ and $L_m = 1000$ m. A more elaborate model has been given by Gossard (6) when the air mass over land is stably stratified.

SUBSIDENCE INVERSIONS

In a high pressure system the frictional outflow of air near the surface is accompanied by a slow subsidence of air from a high level towards the high pressure centre. The surface friction layer forms a base for the subsidence at which marked gradients occur. Temperature increases whilst humidity usually decreases through the inversion because the air from higher levels is very dry. This often causes an elevated duct. Some interesting examples have been given by Flavell (7) and data is given by Dougherty and Hart (8).

CALCULATION OF FIELD STRENGTH

Geometrical Optics

At short distances geometrical optics may be used. For a plane stratified medium Snell's law gives $m(z)\sin\theta = S$ where S is a constant for each ray and θ is the angle to the vertical. Ray tracing methods follow from simple geometry. Figure 4 is an example given by Davies and Evans (9). The ray equations often have multiple solutions giving caustics and cusps where ray theory breaks down. Uniform approximations can be used in these cases but the results are complex. For a transmitter in a surface duct, two kinds of caustics meet in cusps and are designated interior and exterior by Hartree (10), as shown in figure 5.

Waveguide Mode Theory.

Formulation. As shown by Budden (11), the field at greater distances is given by an infinite sum of independently propagating waveguide modes proportional to

$$\frac{1}{D^{\frac{1}{2}}}\sum_{S=S_n} e^{-ik_oSD}\frac{g(z_t,S)g(z_r,S)}{g(0,S)g(0,S)}\left[\frac{\partial w}{\partial S}(0,S)\right]^{-1} \tag{18}$$

where D is range, k_o is the free space wavenumber, z_t and z_r are the terminal heights, and g(z,S) is the height-gain function, the outgoing wave solution of

$$\frac{d^2g(z,S)}{dz^2} = -k_o^2q^2(z,S)g(z,S) = -k_o^2[m^2(z) - S^2]g(z,S) \tag{19}$$

The wave impedance $\varphi(z,S) = \partial\,\ell n\, g(z,S)/\partial z$ satisfies the boundary condition $\varphi(0,S) = ik_o\zeta$ where $\zeta = (n_e^2 - 1)^{\frac{1}{2}}$ for horizontal and $\zeta = (n_e^2 - 1)^{\frac{1}{2}}/n_e^2$ for vertical polarisation with n_e the refractive index of the earth. The solutions are the complex values $S = S_n (n = 1,2,\ldots)$ which are usually ordered by increasing attenuation.

Phase integral and comparison equation methods. For simple problems such as surface ducts, phase integral (WKB) methods may be used. These often give useful analytic approximations. Higher order approximations using the comparison equation method are given by Rotheram (12).

Initial value methods. An iterative initial value method (11) employs the Riccati equation satisfied by the impedance $\varphi(z,S)$ or reflection coefficient $R(z,S) = (ik_oq + \varphi)/(ik_oq - \varphi)$. This satisfies the boundary condition

$$R_o(S)\,R(0,S) = 1 \tag{20}$$

where $R_o(S) = [q(0,S) - \zeta]/[q(0,S) + \zeta]$. A value of S is chosen, R(z,S) is calculated at great heights using the WKB approximation, the Riccati equation is integrated to the surface to give R(0,S), and Newton's method is used to recalculate S from eqn. (20).

Continuation method. Solving eqn. (20) can be quite tricky. It is easy to miss eigenvalues and the initial value of S must be close to S_n. A better method is to define a complex modenumber $\nu(S)$ such that $\nu(S_n) = n$. One such mapping is

$$R_o(S)\,R(0,S) = e^{-2i\varkappa\nu(S)} \tag{21}$$

Solving eqn. (20) amounts to finding $S(\nu)$, the inverse of $\nu(S)$. One technique is to turn eqn. (21) into a differential equation. A value of S is chosen, ν is found from eqn.(21) and the differential equation is integrated numerically to $\nu = 1,2,$ etc. to find S(1), S(2) etc. If $R_o(S)$ or R(0,S) have poles or zeros, the ν-S mapping is not single valued. This

is discussed by Budden (13) in the context of mode degeneracy. Surface duct propagation over a rough surface is an example.

Finite difference methods. Because of these problems a finite difference method is being developed. The infinite height range is transformed to a finite interval by, for example, $x = \exp(-z/z_o)$ where z_o is a suitable scale height. The differential equation and boundary conditions are replaced by finite difference approximations giving a matrix eigenvalue problem. About 10N points must be used to give N accurate eigenvalues for simple m-profiles.

2-dimensional refractive index problems. For the 2 or 3-D problem, coupled mode methods are given by Wait (14) but these are rather complicated. Non-mode methods involving the parabolic wave equation have been used by Tappert (15) in underwater acoustics and these are being studied for radio problems such as the advection duct.

Evaporation duct results. An evaporation duct program has been written using a combination of phase integral, comparison equation, shooting and continuation methods. A rough sea is included by replacing $R_o(S)$ by $R_o(S)\exp[-2k_o^2\sigma^2 q(0,S)^2]$ where σ is the r.m.s. roughness.

Attenuation. This is $\mu_n = .0086\, k_o\, \mathrm{Im}\, S_n$ dB/km for mode number n. Figure 6 shows $(d/10)^{\frac{1}{2}}\mu_1$ plotted against $(d/10)^{3/2} f$ for a series of values of σ/d, with f(GHz) the frequency and d(m) the duct thickness and neutral stability (1/L=0). As f increases, μ_1 decreases as the mode becomes more trapped, but eventually increases because of surface roughness. It tends to a value of about .5 though with an overshoot that for $\sigma/d < .04$ involves an interchange with higher modes, an example of degeneracy (13). For large f the reflected wave is destroyed and the mode structure is as if the earth had been removed.

Height-gain. Figure 7(a) shows $g(S_1,z)/g(S_1 d)$ for neutral stability (1/L=0) and a smooth sea (σ=0) and values of $(d/10)^{3/2} f$ GHz. As this increases the mode becomes trapped and energy concentrates in the duct. Figure 7(b) is for $(d/10)^{3/2} f = 15$ GHz. and roughnesses $\sigma/d = 0, .01, .05$ and .1 showing how the roughness destroys the trapped mode.

Comparison with experiment. Figure 8 shows measurements in the Baltic made by Hamburg University compared with theoretical predictions for neutral stability and various roughnesses. The qualitative features of the data are well predicted.

REFERENCES

1. Monin, A.C. and Obukhov, A.M., 1954, USSR Ac.Sci.Geo.Inst., 24, 162-187.
2. Businger, J.A., Wyngaard, J.C., Izumi, Y. and Bradley, E.F., 1971, J. Atmos.Sci., 18, 181-189.
3. Kondo, J., 1975, Boundary-Layer Met., 9, 91-112.
4. Mulhearn, P.J., 1978, "On surface-based advective radar ducts", RANRL TN5/78.
5. Unwin, R.S., 1051, "Report of Factual Data from the Canterbury Project", Dept. Sci. Ind. Res., Wellington, N.Z.
6. Gossard, E.E. ,1982, Radio Sci., 17, 385-398.
7. Flavell, R.G., 1981, IEE Conf. Publ.,195, 163-167.
8. Dougherty, H.T. and Hart, B.A., 1976, "Anomalous propagation and interference fields", OT Report 76-107.
9. Davies, W.S. and Evans, T.A., 1981, A.T.R., 15, 17-32.
10. Hartree, D.R., 1946, "Meteorological factors in radiowave propagation". The Physical Society, London.
11. Budden, K.G., 1961, "The wave-guide mode theory of wave propagation", Logos Press.
12. Rotheram, S., 1974, Marconi Review, 37, 18-40.
13. Budden, K.G. and Eve, M., 1975, Proc. R.Soc.Lon.A. 342, 175-190.
14. Wait, J.R., 1980, Radio Science, 15, 667-673.
15. Tappert, F.D., 1977, "Wave Propagation and Underwater Acoustics", Ed. by J.B. Keller and J.S. Papadakis. Lecture Notes in Physics Vol. 70. Springer-Verlag.

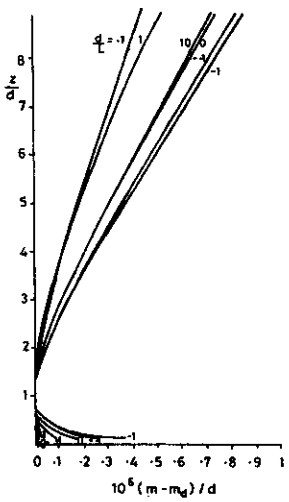

Figure 1 Variation of modified refractive index m with height z, duct thickness d and stability L.

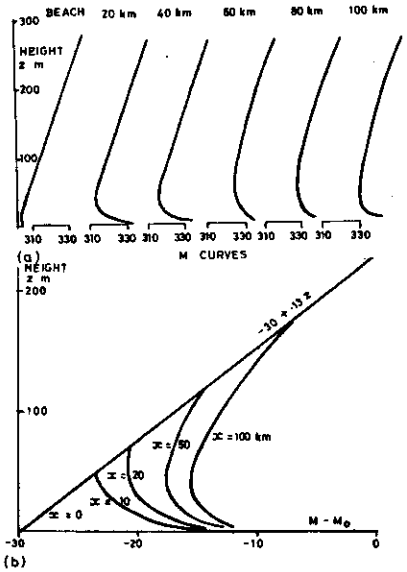

Figure 3 Experimental (a) and theoretical (b) profiles of modified refractivity M.

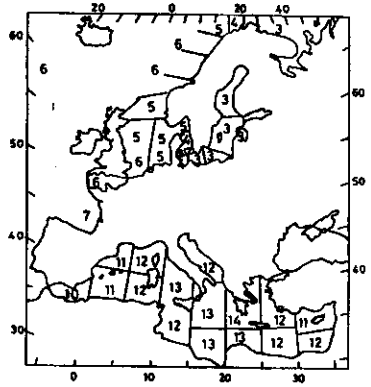

Figure 2 Mean evaporation duct thickness d(m) in European waters.

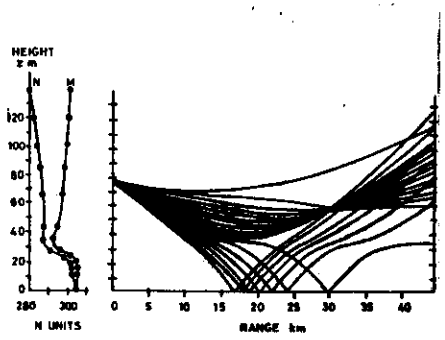

Figure 4 Ray paths in an elevated duct.

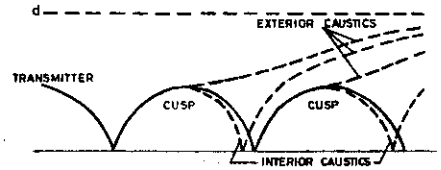

Figure 5 Formation of a set of caustics and cusps in a surface duct.

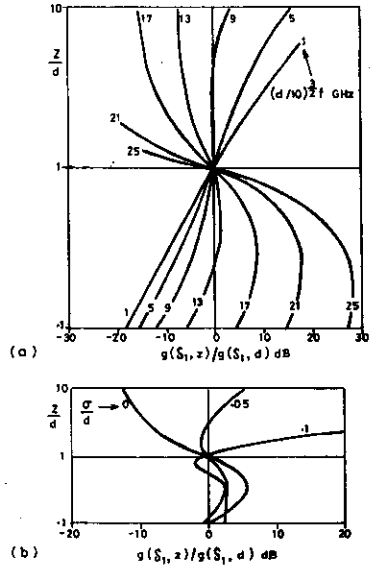

Figure 7 Height-gain functions. Variations with
(a) d(m) & f(GHz) for 1/L=0 & σ=0.
(b) σ for $(d/10)^{3/2}$ f = 15 GHz.

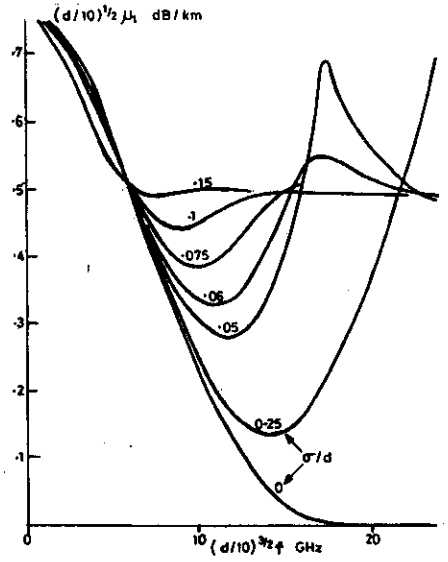

Figure 6 First mode attenuation μ_1(dB/km) as a function of f(GHz), d(m) and σ(m) Neutral stability (1/L=0).

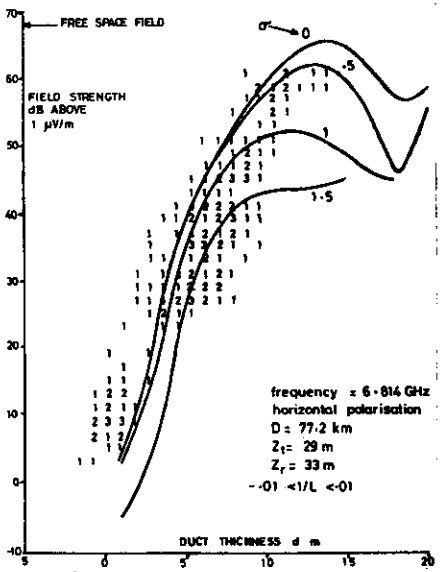

Figure 8 Theoretical and experimental field strength-duct thickness relations for near-neutral stability.